1-2015

Description and Analysis of the Ocean Component of NOAA's Operational Hurricane Weather Research and Forecasting (HWRF) Model

Richard M. Yablonsky

Isaac Ginis
University of Rhode Island, iginis@uri.edu

Biju Thomas

Vijay Tallapragada

Dmitry Sheinin

See next page for additional authors

Citation/Publisher Attribution

Richard M. Yablonsky, Isaac Ginis, Biju Thomas, Vijay Tallapragada, Dmitry Sheinin, and Ligia Bernardet. (2015). "Description and Analysis of the Ocean Component of NOAA's Operational Hurricane Weather Research and Forecasting (HWRF) Model." Journal of Atmospheric and Oceanic Technology, 32, 144-163. Available at: http://dx.doi.org/10.1175/JTECH-D-14-00063.1

Description and Analysis of the Ocean Component of NOAA's Operational Hurricane Weather Research and Forecasting (HWRF) Model

Authors

Richard M. Yablonsky, Isaac Ginis, Biju Thomas, Vijay Tallapragada, Dmitry Sheinin, and Ligia Bernardet

Description and Analysis of the Ocean Component of NOAA's Operational Hurricane Weather Research and Forecasting Model (HWRF)

RICHARD M. YABLONSKY, ISAAC GINIS, AND BIJU THOMAS

Graduate School of Oceanography, University of Rhode Island, Narragansett, Rhode Island

VIJAY TALLAPRAGADA AND DMITRY SHEININ

NOAA/NWS/NCEP/Environmental Modeling Center, College Park, Maryland

LIGIA BERNARDET

NOAA/ESRL/Global Systems Division, and CIRES, University of Colorado Boulder, Boulder, Colorado

(Manuscript received 28 March 2014, in final form 5 September 2014)

ABSTRACT

The Princeton Ocean Model for Tropical Cyclones (POM-TC), a version of the three-dimensional primitive equation numerical ocean model known as the Princeton Ocean Model, was the ocean component of NOAA's operational Hurricane Weather Research and Forecast Model (HWRF) from 2007 to 2013. The coupled HWRF–POM-TC system facilitates accurate tropical cyclone intensity forecasts through proper simulation of the evolving SST field under simulated tropical cyclones. In this study, the 2013 operational version of HWRF is used to analyze the POM-TC ocean temperature response in retrospective HWRF–POM-TC forecasts of Atlantic Hurricanes Earl (2010), Igor (2010), Irene (2011), Isaac (2012), and Leslie (2012) against remotely sensed and in situ SST and subsurface ocean temperature observations. The model generally underestimates the hurricane-induced upper-ocean cooling, particularly far from the storm track, as well as the upwelling and downwelling oscillation in the cold wake, compared with observations. Nonetheless, the timing of the model SST cooling is generally accurate (after accounting for along-track timing errors), and the ocean model's vertical temperature structure is generally in good agreement with observed temperature profiles from airborne expendable bathythermographs.

1. Introduction

The U.S. National Oceanic and Atmospheric Administration (NOAA) Environmental Modeling Center provides real-time tropical cyclone (TC) track and intensity forecast guidance to NOAA's National Hurricane Center. NOAA's Hurricane Weather Research and Forecast Model (HWRF), which is a regional, dynamical TC model, became operational in 2007 after 5 years of development at the Environmental Modeling Center, in collaboration with NOAA's Geophysical Fluid Dynamics Laboratory (GFDL) and the University of Rhode Island. Upgrades to the operational HWRF by the Environmental Modeling Center (with contributions from the wider community), as well as a subsequent community release of the HWRF system by the Developmental Testbed Center (Bernardet et al. 2015), are made on an annual basis. The latest version of HWRF (as of the writing of this manuscript) is the 2013 operational HWRF, version 3.5a, which has three nested atmospheric domains with horizontal grid spacings of 27, 9, and 3 km that employ the Nonhydrostatic Mesoscale Model dynamical core and physical parameterizations of the surface layer, planetary boundary layer, cloud microphysics, deep convection, radiative processes, and land surface, as described in detail in Tallapragada et al. (2013).

The atmospheric component of the HWRF is coupled to a version of the Princeton Ocean Model (POM; Mellor 2004). The primary purpose of coupling an ocean model to a TC model (such as HWRF or GFDL) is to create an accurate sea surface temperature (SST) field, particularly

Corresponding author address: Richard M. Yablonsky, Graduate School of Oceanography, University of Rhode Island, Box 67, 215 South Ferry Rd., Narragansett, RI 02882.
E-mail: rmyablon@mail.uri.edu

DOI: 10.1175/JTECH-D-14-00063.1

in the storm core. This SST field is subsequently used by the TC model to calculate the surface heat and moisture fluxes from the ocean to the atmosphere. Many modeling studies have highlighted the importance of TC–ocean model coupling for simulating TC intensity, including idealized case studies (Ginis et al. 1989; Bender et al. 1993; Hodur 1997; Schade and Emanuel 1999; Bao et al. 2000; Chan et al. 2001; Wu et al. 2005; Wu et al. 2007; Liu et al. 2011; Yablonsky and Ginis 2013), as well as real-case studies in the North Atlantic (Bender and Ginis 2000; Hong et al. 2000; Emanuel et al. 2004; Chen et al. 2007; Wu et al. 2007; Sanabia et al. 2013; Kim et al. 2014), western North Pacific (Lin et al. 2005; Wu et al. 2007), and South Pacific Oceans (Sandery et al. 2010; Jullien et al. 2014). The primary conclusion from these modeling studies is that an uncoupled TC model with a static SST field is restricted by its inability to account for TC-induced SST cooling during TC model integration, which can cause an overestimate of the surface heat and moisture fluxes in the storm core and contribute to a high-intensity bias.

An accurate SST field requires ocean physics that can generate accurate SST change in response to wind (and to a lesser extent, thermal) forcing at the air–sea interface. SST change induced by wind forcing is primarily due to vertical mixing and entrainment in the upper ocean. Vertical mixing occurs because wind stress generates ocean surface layer currents, and the resulting vertical current shear leads to turbulence, which then mixes the upper ocean and entrains colder water from the thermocline up into the well-mixed ocean surface layer, ultimately cooling the SST (e.g., Price 1981; Shay et al. 1989; Jacob et al. 2000; Ginis 2002; Jullien et al. 2012; Vincent et al. 2012a). In addition, the cyclonic wind stress induced by a hurricane creates divergent surface currents in the upper ocean, thereby causing upwelling of cooler water from the thermocline toward the sea surface. For slow-moving storms, this upwelling increases the efficiency with which vertical mixing can entrain cooler water from the thermocline into the well-mixed ocean surface layer, ultimately cooling the SST (Price 1981; Yablonsky and Ginis 2009). Finally, horizontal advection may impact the SST distribution, especially in oceanic fronts and eddies, where strong background currents exist (D'Asaro 2003; Jacob and Shay 2003; Huang et al. 2009; Jaimes and Shay 2009; Yablonsky and Ginis 2013). Hence, both the HWRF and GFDL models are coupled to a fully three-dimensional version of POM, called POM for Tropical Cyclones (POM-TC). The remainder of this manuscript includes a brief description of the POM-TC component of the 2013 operational HWRF used to forecast TC track and intensity, as well as an ocean model–based analysis of selected HWRF–POM-TC simulations.

2. POM-TC description

The full POM-TC model description can be found in 2013 HWRF scientific documentation (Tallapragada et al. 2013). Here, a brief history of the model and a summary of its main features are provided. The three-dimensional primitive equation numerical ocean model known as POM was originally developed at Princeton in the late 1970s (Mellor 2004). In 1994, a version of POM available at the time was transferred to the University of Rhode Island for the purpose of coupling to the GFDL hurricane model. At this point, POM code changes were made specifically to address the problem of the ocean's response to hurricane wind forcing in order to create a more realistic SST field for input into the hurricane model. Initial testing showed hurricane intensity forecast improvements when ocean coupling was included (Bender and Ginis 2000). Since operational implementation of the coupled GFDL–POM model at NOAA in 2001, additional changes to POM were made at the University of Rhode Island and subsequently implemented in the operational GFDL model, including improved ocean initialization (Falkovich et al. 2005; Bender et al. 2007; Yablonsky and Ginis 2008). This POM version was then coupled to the atmospheric component of the HWRF before operational implementation of HWRF at NOAA in 2007.

a. POM-TC configuration

The horizontal POM-TC grid uses curvilinear orthogonal coordinates, and spatial differencing of the POM-TC variables is done on the staggered Arakawa C grid, so some model variables are calculated at a horizontally shifted location from other model variables (Mellor 2004, section 4). There are two overlapping grids in the North Atlantic Ocean, both of which are bounded by 10°N latitude to the south and 47.5°N to the north (Fig. 1). The first grid covers the Gulf of Mexico, Caribbean, and west Atlantic region (the "United" region), which is bounded by 98.5°W longitude to the west and 50°W longitude to the east. The second grid covers the east Atlantic region, which is bounded by 60°W longitude to the west and 30°W longitude to the east. HWRF uses the current and 72-h forward-extrapolated storm track to choose which grid to use for coupling. Both grids are configured with ~18-km grid spacing in the latitudinal and longitudinal directions. Although this horizontal resolution is arguably too coarse for TC simulations, it is selected to reduce the run time of the ocean model to comply with NOAA's operational requirements, which are further constrained by the fact that POM-TC runs on one processor. Nonetheless, POM-TC is able to capture the magnitude and spatial

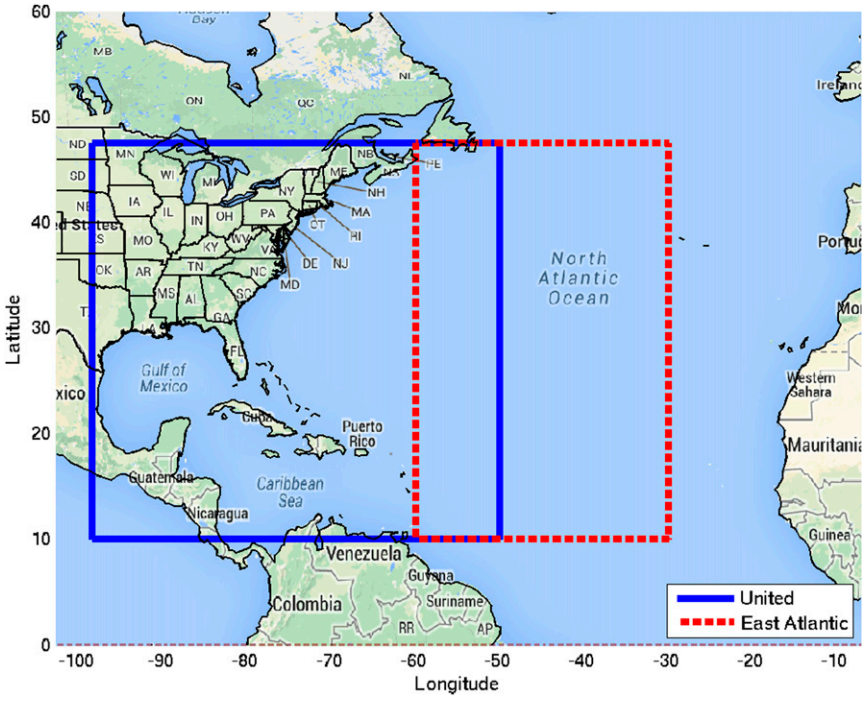

FIG. 1. HWRF–POM-TC United (blue solid) and east Atlantic (red dashed) ocean regions.

distribution of SST cooling due to TC forcing with reasonable accuracy, as shown in section 3.

The vertical coordinate is the terrain-following sigma coordinate system (Phillips 1957; Mellor 2004, Fig. 1 and appendix D). There are 23 vertical levels, where the level placement is scaled based on the bathymetry of the ocean at a given location; the largest vertical spacing occurs where the ocean depth is 5500 m. Here, the 23 half-sigma vertical levels are located at depths of 5, 15, 25, 35, 45, 55, 65, 77.5, 92.5, 110, 135, 175, 250, 375, 550, 775, 1100, 1550, 2100, 2800, 3700, 4850, and 5500 m.

POM-TC has a free surface and a split time step. The internal mode is three-dimensional and uses a 9-min time step during coupled POM-TC integration. Horizontal time differencing is explicit, but vertical time differencing is implicit, eliminating time constraints for the vertical coordinate and permitting high vertical resolution in the surface boundary layer (Mellor 2004, section 4).

Turbulence in POM-TC is parameterized using the Mellor–Yamada level 2.5 turbulence closure model, which provides vertical mixing coefficients (Mellor and Yamada 1982; Mellor 2004, sections 1 and 14). Smagorinsky (1963) diffusivity is used for horizontal diffusion.

b. POM-TC initialization

Prior to coupled model integration of the HWRF–POM-TC, POM-TC is initialized with realistic three-dimensional temperature and salinity fields and subsequently integrated to generate realistic ocean currents and to incorporate the preexisting hurricane-generated cold wake. The starting point for the ocean initialization is the Generalized Digital Environmental Model (GDEM) monthly ocean temperature and salinity climatology (Teague et al. 1990), which has ½° horizontal grid spacing and 33 vertical z levels. In the United region, the GDEM climatology is then modified diagnostically by interpolating it in time to the POM-TC initialization date (using 2 months of GDEM), horizontally interpolating it onto the POM-TC United grid, incorporating a land–sea mask and bathymetry data, and employing a feature-based modeling procedure that incorporates historical and near-real-time observations of prominent ocean fronts and eddies (Falkovich et al. 2005; Yablonsky and Ginis 2008). In the east Atlantic region, the diagnostic modifications to the GDEM climatology are similar, but the feature-based modeling procedure is not used because there are no major fronts or eddies in this region.

The basic premise of the feature-based modeling procedure is that major oceanic fronts and eddies in the western North Atlantic Ocean—namely, the Gulf Stream, the Loop Current, and eddies associated with the Loop Current—are poorly represented by the GDEM climatology's temperature and salinity fields. By defining the spatial structure of these fronts and eddies using historical observations gathered from various field experiments (Falkovich et al. 2005, section 3), cross-frontal "sharpening" of the

GDEM temperature and salinity fields can be performed to obtain more realistic fields by increasing the horizontal density gradients across the fronts. These sharpened fields yield stronger geostrophically adjusted ocean currents along the front than would be obtained directly from GDEM. In addition, algorithms were incorporated into the feature-based modeling procedure to initialize the Gulf Stream and Loop Current with prescribed paths and to insert eddies into the Gulf of Mexico based on guidance from near-real-time observations, such as satellite altimetry (Yablonsky and Ginis 2008, section 2).

After the aforementioned diagnostic modifications to the GDEM climatology (including the feature-based modifications in the United region), at the beginning of what is referred to as ocean spinup "phase 1," the upper-ocean temperature field is modified by assimilating the real-time daily SST data (with 1° grid spacing) that is used in NOAA's operational Global Forecast System analysis (Reynolds and Smith 1994). While this SST product has relatively coarse resolution, it is chosen instead of other higher-resolution SST products to ensure consistency near the air–sea interface between the ocean initialization and the atmospheric initialization, the latter of which also uses the NOAA's operational Global Forecast System analysis. Further details of the SST assimilation procedure can be found in Yablonsky and Ginis (2008, section 2). Finally, the three-dimensional temperature and salinity fields are interpolated from the GDEM z levels onto the POM-TC vertical sigma levels, and the density is calculated using the modified United Nations Educational, Scientific, and Cultural Organization equation of state (Mellor 1991), ending the diagnostic portion of the ocean initialization.

Ocean spinup phase 1 involves 48 h of POM-TC integration, primarily for dynamic adjustment of the density field and generation of dynamically consistent currents. During phase 1, SST is held constant. Once phase 1 is complete, the phase 1 output is used to initialize ocean spinup "phase 2." During phase 2, the cold wake at the ocean surface and the currents produced by the hurricane prior to the beginning of the coupled model forecast are generated by a 72-h integration of POM-TC with the observed hurricane surface wind distribution provided by NOAA's National Hurricane Center along the storm track. This surface wind distribution is based on interpolation of the radial wind profiles derived from the storm message file (Bender and Ginis 2000), also known as the TC vitals (Trahan and Sparling 2012). The storm message file contains the storm position, propagation speed and direction, central and environmental pressure, radius of outermost closed isobar, maximum wind speed, radius of maximum wind, and radii of 17, 26, and 33 m s^{-1} winds in the northeast, southeast, southwest, and northwest quadrants of the storm, when available. Once phase 2 is complete, the phase 2 output is used to initialize the POM-TC component of the coupled HWRF.

c. *POM-TC coupling to the HWRF atmosphere*

The atmosphere–ocean coupler is designed as an independent interface between POM-TC and the HWRF atmospheric component. At every internal ocean time step (9 min), which is synchronized with an atmospheric time step, the instantaneous SST is passed from the ocean to the HWRF atmosphere, and the time-averaged total heat and momentum fluxes at the air–sea interface (over all atmospheric time steps between the previous internal ocean time step and the current one) are passed from the atmosphere to the ocean. Freshwater fluxes are not exchanged across the air–sea interface, although Jourdain et al. (2013) suggest that heavy rainfall may have a nonnegligible impact on the ocean response to TCs in some cases. The coupler serves as a hub for communications between the HWRF atmosphere and POM-TC; it performs the interpolation of the surface fluxes from the fixed and moving HWRF atmospheric grids to the POM-TC grid, and it performs the interpolation of the SST from the POM-TC grid to the two outermost HWRF atmospheric grids. A generalized bilinear interpolation for nonrectangular quadrilateral grid cells is used; only sea-point values of the surface fields are employed for the interpolation.

3. Retrospective 2013 version HWRF–POM-TC model forecast analysis

Since the operational HWRF–POM-TC is upgraded annually, its track and intensity skill, as well as its skill at forecasting storm size, has improved over time. The highest skill through 2013 was achieved by the 2013 operational version (Tallapragada et al. 2013), based on analysis of a homogeneous and statistically robust set of retrospective forecasts from the 2010–12 Atlantic hurricane seasons, which includes 1022, 930, 833, 745, 660, 575, 515, 454, 403, 354, and 314 forecasts at lead times of 0, 12, 24, 36, 48, 60, 72, 84, 96, 108, and 120 h, respectively (Fig. 2). These retrospective HWRF–POM-TC forecasts (identified simply as "HWRF" when referring to either the atmospheric or the oceanic component of the model) provide an opportunity to analyze the POM-TC ocean response using a state-of-the-art version of HWRF. Here, the focus is on specific HWRF forecast cycles from Hurricanes Earl (2010), Igor (2010), Irene (2011), Isaac (2012), and Leslie (2012) in which the accuracy of the hurricane track (Marchok 2002), intensity, and size were

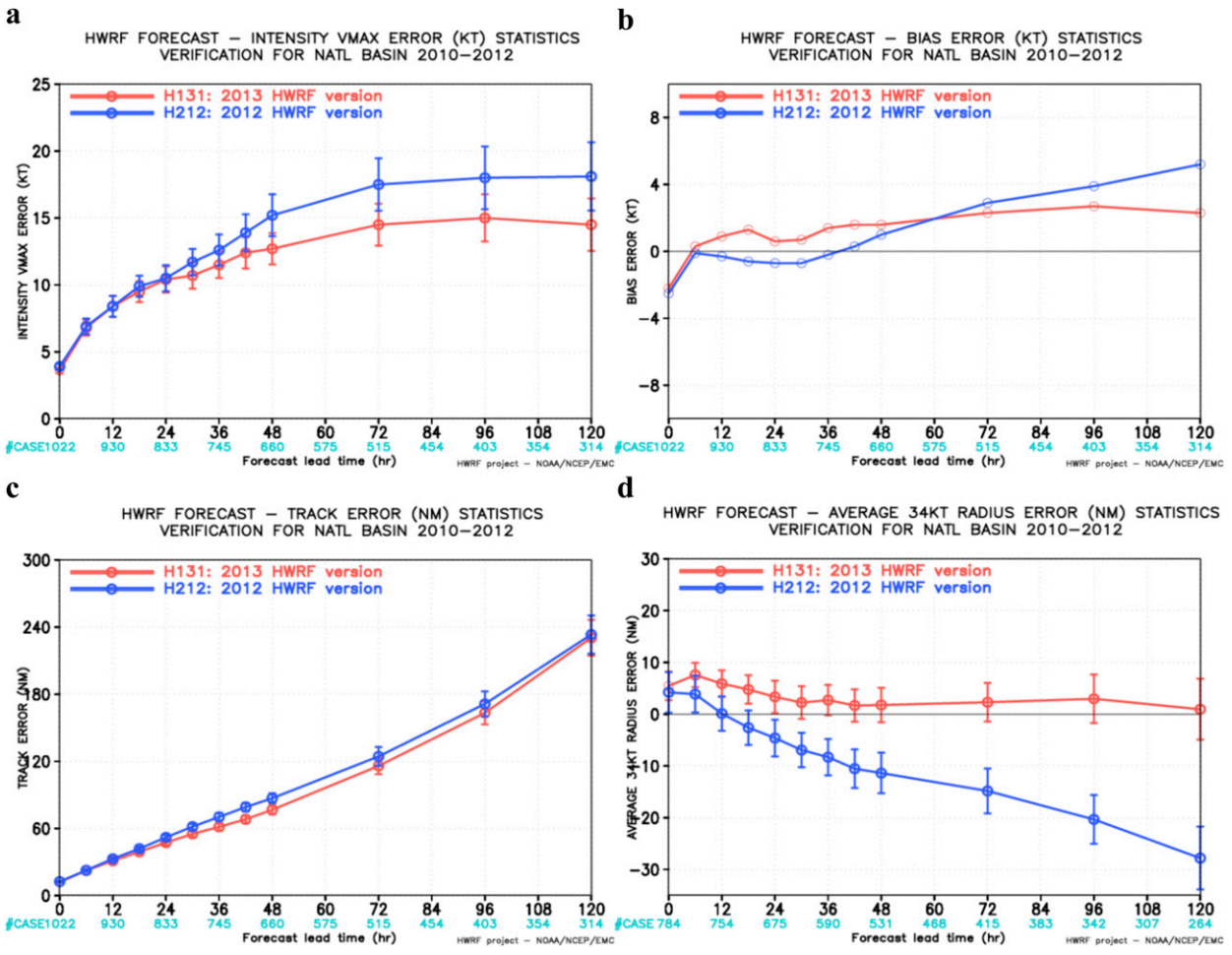

FIG. 2. Average TC intensity (a) error and (b) bias (kt; 1 kt = 0.51 m s^{-1}), as well as (c) track error and (d) average 17 m s^{-1} (34 kt) wind radius bias (nm), as a function of forecast lead time (h) from a homogeneous comparison of the 2013 operational HWRF–POM-TC version (H131, red) to the 2012 operational HWRF–POM-TC version (H212, blue) for all 2010–12 Atlantic TCs, which includes 1022, 930, 833, 745, 660, 575, 515, 454, 403, 354, and 314 forecasts at lead times of 0, 12, 24, 36, 48, 60, 72, 84, 96, 108, and 120 h, respectively.

sufficient, relative to the National Hurricane Center best track (Avila 2002), to analyze the POM-TC SST (and subsurface ocean temperature for the Irene case) using remotely sensed and in situ SST and subsurface temperature observations, when available. This analysis strategy is chosen instead of a comprehensive, statistical ocean analysis of all 2010–12 forecasts, which is more appropriate when the TC parameters (track, intensity, and size) are based on an atmospheric (re)analysis instead of a forecast (e.g., Vincent et al. 2012a,b; Mei and Pasquero 2013; Jourdain et al. 2014).

a. HWRF–POM-TC sea surface temperature analysis

In this section, the SST cooling produced during HWRF coupled model integration is compared to remotely sensed and in situ SST observations to assess how well POM-TC captures the SST cooling. There are two challenges that exist when performing such an analysis: 1) an observational SST data source must be available that indicates the location, magnitude, and spatial extent of the TC cold wake during or shortly after storm passage; and 2) the HWRF-forecasted TC track, propagation speed, intensity, and size must be sufficiently accurate to ensure that cross-track errors, along-track propagation speed errors, intensity errors, and/or size errors do not significantly bias the POM-TC SST response relative to the observations. One reasonably reliable data source that addresses the first challenge is the satellite-derived 3-day averaged SST from the Tropical Rainfall Measuring Mission Microwave Imager (TMI; Gentemann et al. 2004, 2010). Since microwave SST products (including TMI) do not provide reliable estimates under heavy rainfall (Wentz et al. 2000), the 3-day averaged TMI SST is used instead of the daily TMI SST to ensure adequate spatial coverage during storm passage, perhaps at the expense of higher temporal resolution. One

way to address the second challenge is to select specific TCs during specific forecast cycles when the aforementioned TC parameters are well forecasted (in addition to producing a relatively large ocean response). Perhaps not surprisingly, during analysis of the POM-TC SST response in the HWRF–POM-TC coupled system in which the aforementioned TC parameters were *not* well forecasted, biases in the HWRF atmospheric component have been identified over the years, often leading to specific improvements in the HWRF atmospheric component that at first glance may appear to be independent of the ocean response.

The HWRF coupled model forecast of Hurricane Earl, initialized at 0600 UTC 30 August 2010, is shown in Fig. 3, with the first ~12 h and the final ~6 h of the forecast track cut off in order to zoom in on the cold wake produced by the model forecast. The HWRF cold wake SST at forecast hour 120 (Fig. 3a), and hence the HWRF cold wake SST anomaly at forecast hour 120 relative to forecast hour 0 (Fig. 3c), is up to ~2°C warmer than the observed cold wake SST from the 3-day averaged (2–4 September) TMI SST product (Figs. 3b,d). In addition, the spatial extent of the HWRF cold wake is only about half as wide as in the TMI in many locations, particularly during the first 84 h of the forecast. Examining the HWRF temperature at 77.5-m depth (Fig. 3e) reveals that Earl propagated along the boundary between areas of higher ocean heat content to the south and west and lower ocean heat content to the north and east, the detailed structure of which could impact the magnitude of the cold wake. In addition, the HWRF intensity was generally ~10 m s^{-1} weaker than observed during the first 84 h of the forecast (Fig. 3f), which likely contributed to the undercooling in the HWRF forecast relative to observations. However, the HWRF storm size, as indicated by the radius of the 17 m s^{-1} wind, is within 50 km of the observed storm size during the first 96 h of the forecast (Fig. 3f), so storm size errors do not explain the underforecasted spatial extent of the cold wake.

Two buoys located close to Earl's track provide an opportunity to compare the temporal evolution of the HWRF SST to observations at point locations. At NOAA National Data Buoy Center (NDBC) buoy 41001, located east of Earl's center at forecast hour ~96–102, the HWRF SST is ~1°C warmer than the buoy SST at the initial time. Assuming the buoy SST is accurate, this result indicates that the blended, coarse-resolution Global Forecast System SST analysis, which is assimilated into the HWRF–POM-TC initial condition, is ~1°C too warm at the buoy location. The magnitude of the HWRF SST cooling from forecast hour ~96 to ~108 is similar to the buoy SST cooling, with a 3–6-h phase lag in the HWRF SST relative to the buoy SST (Fig. 3g), due to the slower HWRF storm propagation speed relative to the best track (Figs. 3a–e). Also, given the phase lag and the fact that the HWRF forecast ends at hour 120, it is not clear whether the continued cooling observed by the buoy after the short recovery (forecast hour ~108 and beyond) is also captured by the HWRF forecast. At NOAA NDBC buoy 41046, located northeast of Earl's center at forecast hour ~42, the HWRF SST cooling is underestimated by ~1°C during storm passage (forecast hour ~36–48), but the more significant HWRF SST cooling underestimation occurs later during subsequent upwelling cycles (forecast hour 60 and beyond) (Fig. 3h). Since Earl was propagating rather quickly (~6–7 m s^{-1}), this "poststorm" underestimation of SST cooling is unlikely to have played a significant role in Earl's HWRF forecast intensity bias. Note that in Figs. 3g,h, the SSTs from nearby HWRF ocean model grid points are shown in addition to the SST from the closest model grid point to illustrate errors that may be introduced by insufficient ocean model horizontal resolution.

The underforecasted magnitude of Earl's cold wake may be attributable to a number of other factors, including insufficient ocean model resolution, limitations in the parameterization of the upper-ocean mixing, underestimation of the heat and momentum fluxes at the sea surface, and/or misrepresentation of the initial ocean temperature (and perhaps salinity) structure. For example, the erroneously warm Global Forecast System SST assimilated into the ocean model may have led to an unrealistically stable upper-ocean temperature profile, which could have reduced the entrainment rate at the base of the upper-ocean mixed layer. Also, Vincent et al. (2012a) have shown that the magnitude of the SST cooling in periphery of the storm is particularly sensitive to the air–sea heat flux.

The HWRF 120-h coupled model forecast of Hurricane Igor, initialized at 0000 UTC 15 September 2010, is shown in Fig. 4. Similar to Earl, the Igor HWRF cold wake SST at forecast hour 120 (Figs. 4a,c) is up to 2°–3°C warmer than the observed cold wake SST from the 3-day averaged (18–20 September) TMI SST product (Figs. 4b,d), and the spatial extent of the cold wake is only about half as wide as in the TMI along the second half of the forecast track. Examining the HWRF temperature at 77.5-m depth (Fig. 4e) reveals that Igor propagated northward across a boundary of higher ocean heat content to the south and lower ocean heat content to the north, the detailed structure of which again could impact the magnitude of the cold wake. Throughout the forecast, the HWRF intensity was within 5–10 m s^{-1} of the best track, and the HWRF storm size was within 50 km of the best track observations (Fig. 4f), so intensity and size

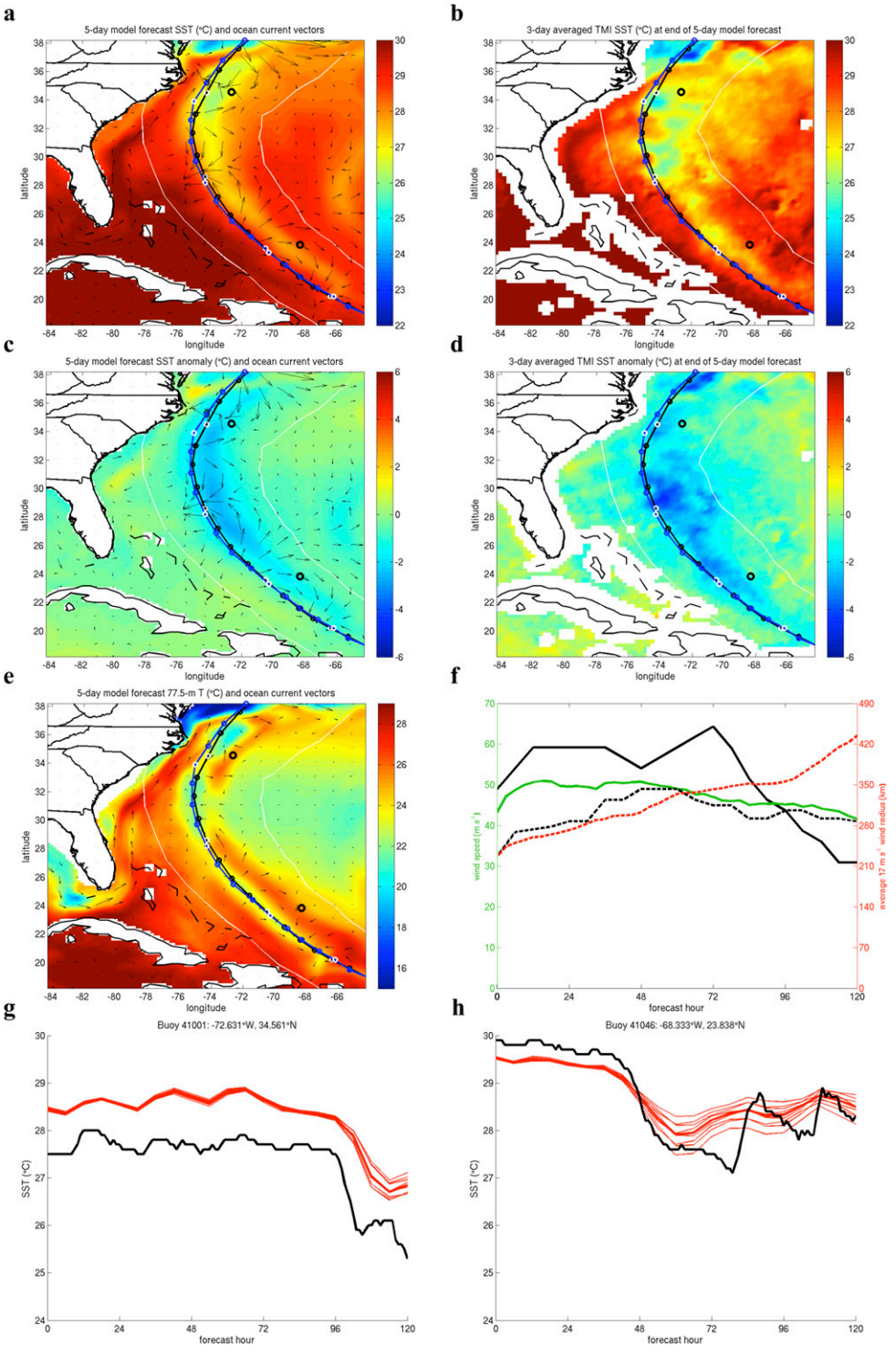

FIG. 3. HWRF–POM-TC forecast of Hurricane Earl, initialized 0600 UTC 30 Aug 2010: (a) 120-h model SST and current with model track (blue with white circles every 24 h), model 17 m s^{-1} wind swath (white), best track (black), and two buoys (black rings); (b) 2–4 Sep TMI SST with best track 17 m s^{-1} wind swath (white); (c) 120-h model SST anomaly; (d) 2–4 Sep TMI SST anomaly from 28 to 30 Aug; (e) 120-h model 77.5-m temperature *T*; (f) maximum wind from model (green) and observed (black), and 17 m s^{-1} wind radius from model (red dashed) and observed (black dashed); (g) buoy 41001 SST (black) with collocated (thick red) and nearby (thin red) model SST; (h) as in (g), but for buoy 41046.

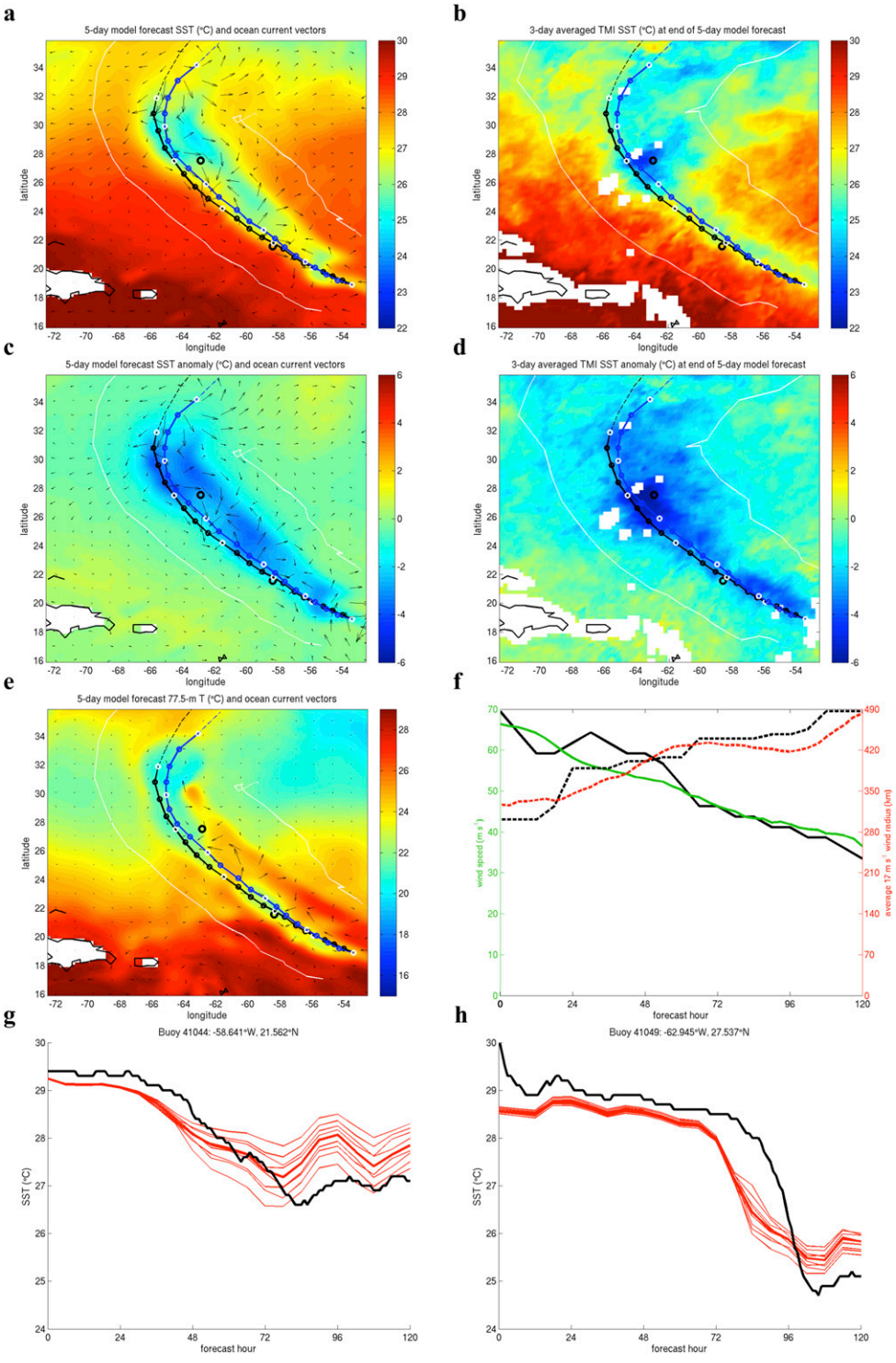

FIG. 4. HWRF–POM-TC forecast of Hurricane Igor, initialized 0000 UTC 15 Sep 2010: (a) 120-h model SST and current with model track (blue with white circles every 24 h), model 17 m s^{-1} wind swath (white), best track (black), and two buoys (black rings); (b) 18–20 Sep TMI SST with best track 17 m s^{-1} wind swath (white); (c) 120-h model SST anomaly; (d) 18–20 Sep TMI SST anomaly from 13 to 15 Sep; (e) 120-h model 77.5-m *T*; (f) as in Fig. 3f; (g) buoy 41044 SST (black) with collocated (thick red) and nearby (thin red) model SST; (h) as in (g), but for buoy 41049.

errors do not account for the underestimation of the magnitude or spatial extent of Igor's SST cooling. As in Earl, this underestimation could be due to errors in the initial ocean condition and/or shortcomings in the ocean model. The particularly large differences between the model and observed cooling at the end of the forecast, however, may also be impacted by the coarse temporal resolution in the 3-day averaged TMI SST product.

Two buoys located close to Igor's track provide an opportunity to compare the temporal evolution of the HWRF SST to observations at point locations. At NOAA NDBC buoy 41044, located near Igor's center at HWRF forecast hour ~42 (observed hour ~48), the magnitude of the HWRF SST cooling is generally underestimated by ~0.5°–1°C relative to the buoy SST cooling, with a phase lag of ~6 h in the buoy SST relative to the HWRF SST (Fig. 4g) due to the faster HWRF storm propagation speed relative to the best track (Figs. 4a–e). The fast HWRF storm propagation speed may at least partially explain the underestimated HWRF SST cooling. Also, the large spread at nearby grid points indicates the strong sensitivity of the buoy location relative to the storm track, which is not surprising because the cold wake is strongly biased to the right of the storm track with a sharp SST gradient across the storm track. At NOAA NDBC buoy 41049, located northeast of Igor's center at HWRF forecast hour ~78 (observed hour ~90), the HWRF SST cooling is again generally underestimated by ~0.5°–1°C relative to the buoy SST cooling, with a phase lag of ~12 h in the buoy SST relative to the HWRF SST due to the faster HWRF storm propagation speed relative to the best track (Fig. 4h).

The HWRF 120-h coupled model forecast of Hurricane Irene, initialized at 1200 UTC 23 August 2011, is shown in Fig. 5. More dramatic than either Earl or Igor, the Irene HWRF cold wake SST at forecast hour 120 (Figs. 5a,c) is up to 3°–4°C warmer than the observed cold wake SST from the 3-day averaged (26–28 August) TMI SST product (Figs. 5b,d). Examining the HWRF temperature at 77.5-m depth (Fig. 5e) reveals that Irene was east of the Gulf Stream until it reached ~32°–33°N, at which point Irene's center crossed the Gulf Stream ~6–12 h before making landfall along North Carolina's east coast. Along the second half of the forecast track, where the difference between the model and observed SST is largest (Figs. 5a–d), the HWRF intensity is up to ~10 m s^{-1} *higher* than the best track, and the HWRF storm size is generally within 50 km of the best track (Fig. 5f); so again, neither intensity nor size errors explain the SST cooling errors. In section 3b, the cold wake during this Irene forecast is examined in more detail by comparing the subsurface temperature evolution against profiles from airborne expendable bathythermograph (AXBT) instruments and considering the bathymetry (Figs. 5g,h; 8; 9). As in the previous cases, however, it is possible that ocean-to-atmosphere heat flux is systematically underestimated in the model, the diagnosis of which would require observations of air–sea fluxes that are not currently available.

The HWRF 48-h coupled model forecast of Hurricane Isaac, initialized at 1200 UTC 27 August 2012, is shown in Fig. 6. The magnitude of the Isaac HWRF cold wake at forecast hour 48 (Figs. 6a,c) is underestimated relative to the observed cold wake SST from the 3-day averaged (27–29 August) TMI SST product (Figs. 6b,d) along the first half of the forecast track, but it is overestimated along the second half of the forecast track. The cold wake differences along the first half of the track may be influenced by subtle differences between the HWRF representation (Figs. 6e,g) and the observed characteristics [based on the sea surface height (SSH) derived from satellite altimetry] (Fig. 6h) of the warm and cold ocean eddies north of the Loop Current in the vicinity of Isaac's track; subsurface observed temperature profiles would be required to examine this hypothesis in more detail (e.g., Yablonsky and Ginis 2008). The apparent overestimation along the second half of the track may in fact not be an overestimation but rather a limitation of the 3-day temporal averaging technique used to generate the TMI SST, particularly close to the coast; indeed, examination of the 3-day averaged TMI SST from the following day (28–30 August) indicates larger observed cooling (not shown), consistent with the HWRF forecast. In addition, the HWRF intensity is ~5–10 m s^{-1} higher than the best track shortly before landfall, although the HWRF storm size is up to ~50 km smaller than the best track at this time (Fig. 6f).

The HWRF 120-h coupled model forecast of Hurricane Leslie, initialized at 0000 UTC 3 September 2012, is shown in Fig. 7. Unlike Earl, Igor, Irene, and Isaac, Leslie was a very slow-moving storm during a large part of its life cycle, allowing for intense upwelling and SST cooling underneath storm core, which certainly limited the storm's intensity. Nonetheless, like the other storms, the magnitude and spatial extent of the Leslie HWRF cold wake SST at forecast hour 120 (Figs. 7a,c) is not as large as the observed cold wake SST from the 3-day averaged (6–8 September) TMI SST product (Figs. 7b,d). Examining the HWRF temperature at 77.5-m depth (Fig. 7e) reveals that Leslie propagated northward across a boundary of higher ocean heat content to the south and lower ocean heat content to the north, the detailed structure of which yet again could impact the magnitude of the cold wake. The HWRF intensity forecast is generally 5–10 m s^{-1} higher, and the HWRF

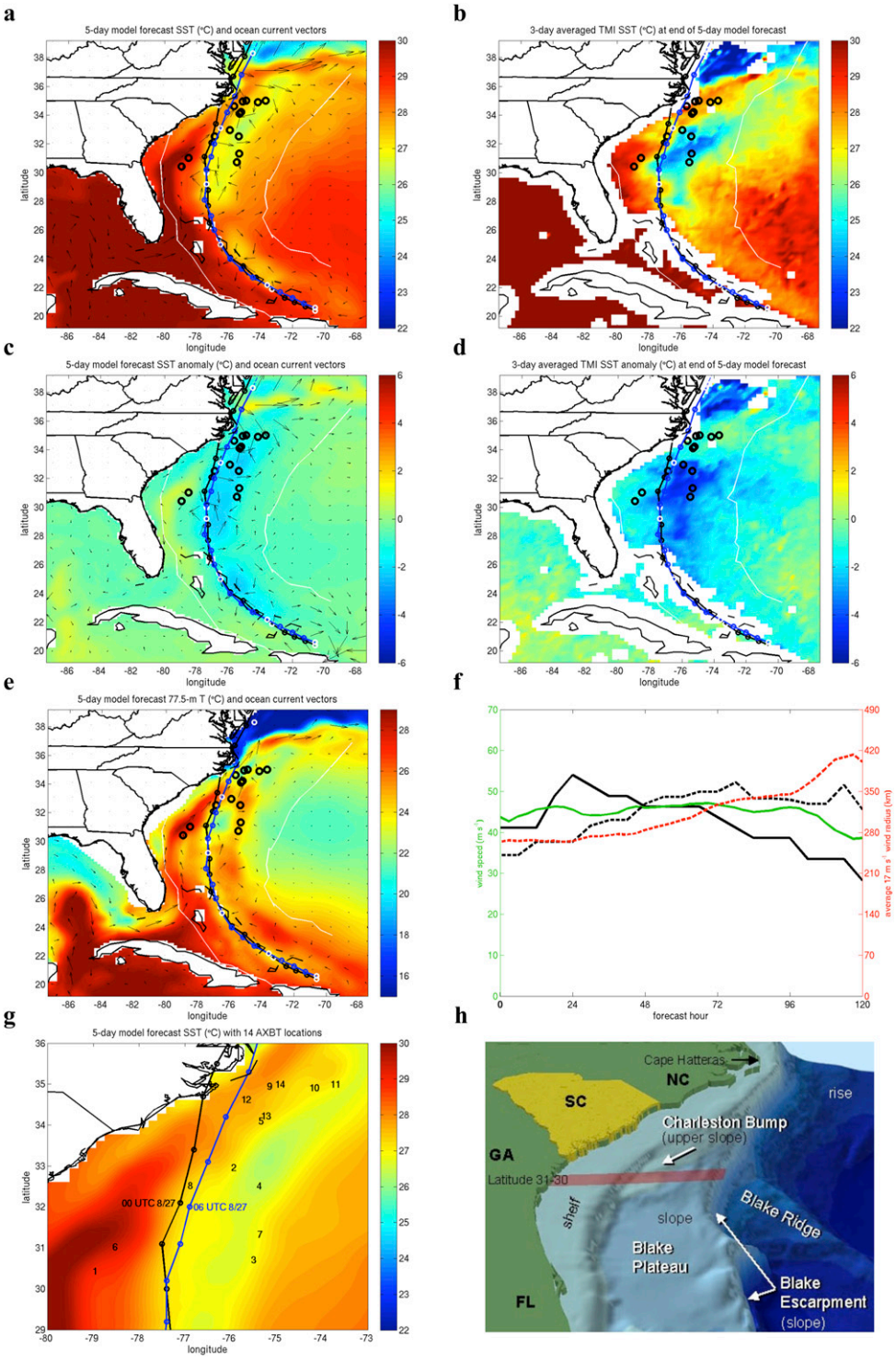

FIG. 5. HWRF–POM-TC 120-h forecast of Hurricane Irene, initialized 1200 UTC 23 Aug 2011: (a) 120-h model SST and current with model track (blue with white circles every 24 h), model 17 m s^{-1} wind swath (white), best track (black), and 14 AXBTs (black rings); (b) 26–28 Aug TMI SST with best track 17 m s^{-1} wind swath (white); (c) 120-h model SST anomaly; (d) 26–28 Aug TMI SST anomaly from 21 to 23 Aug; (e) 120-h model 77.5-m T; (f) as in Fig. 3f; (g) 120-h model SST zoomed in on 26–28 Aug with 6-h model/best tracks and AXBTs numbered 1–14; (h) diagram of the continental shelf and slope of the southeastern United States (courtesy of NOAA).

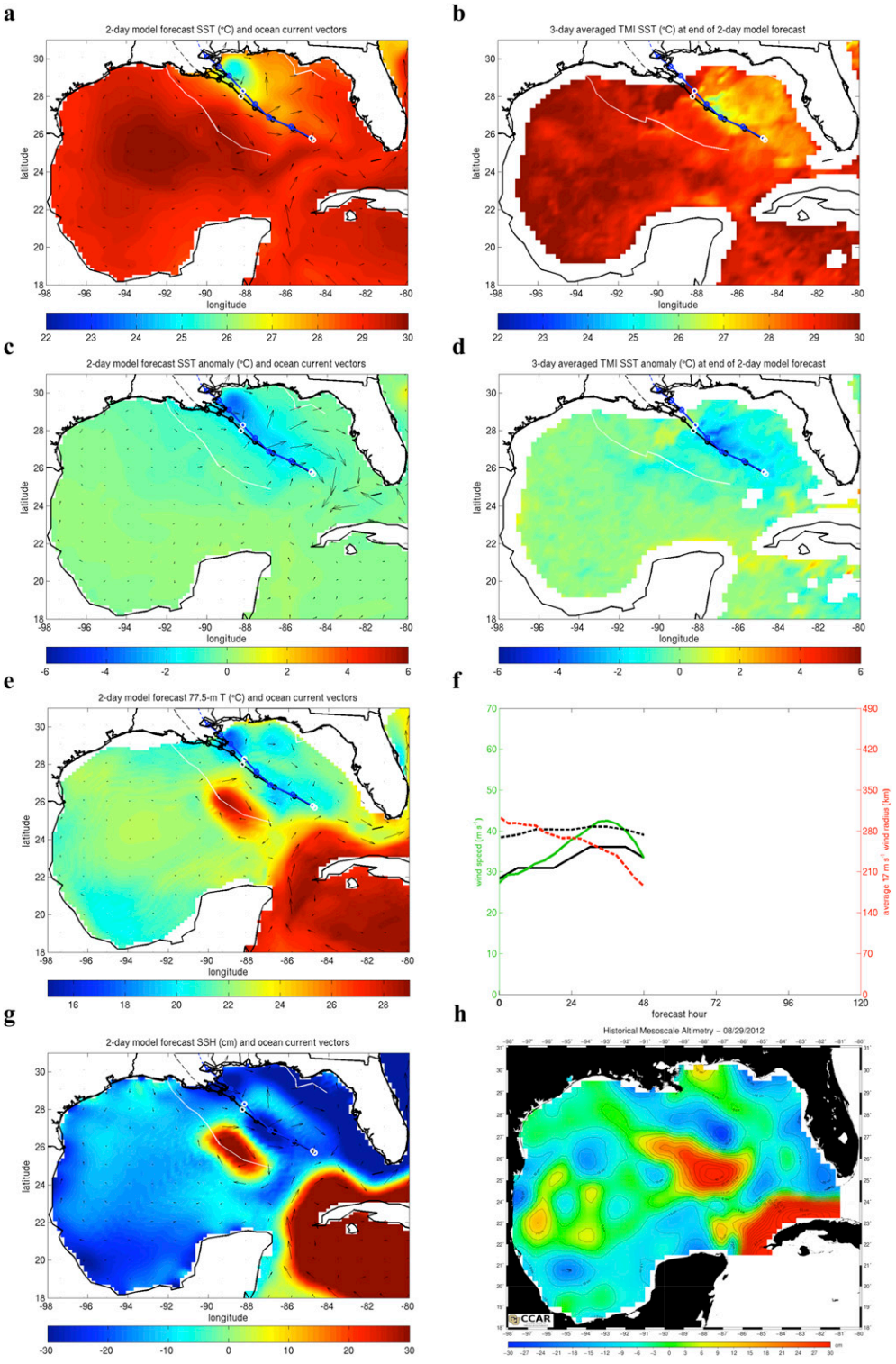

FIG. 6. HWRF–POM-TC 48-h forecast of Hurricane Isaac, initialized 1200 UTC 27 Aug 2012: (a) 48-h model SST and current with model track (blue with white circles every 24 h), model 17 m s^{-1} wind swath (white), and best track (black); (b) 27–29 Aug TMI SST with best track 17 m s^{-1} wind swath (white); (c) 48-h model SST anomaly; (d) 27–29 Aug TMI SST anomaly from 25 to 27 Aug; (e) 48-h model 77.5-m *T*; (f) as in Fig. 3f; (g) 48-h model SSH; (h) 29 Aug satellite-derived SSH.

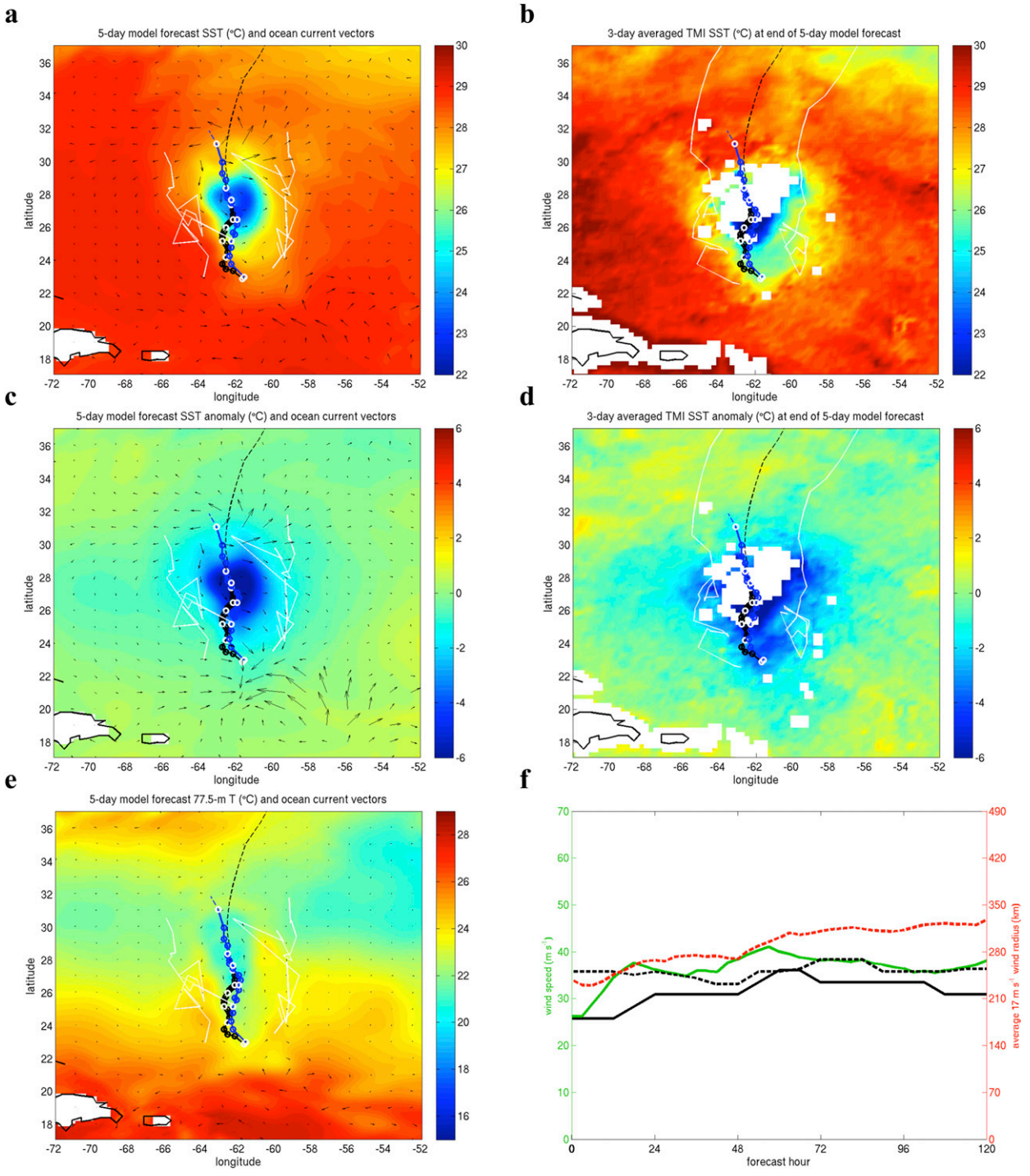

FIG. 7. HWRF–POM-TC forecast of Hurricane Leslie, initialized 0000 UTC 3 Sep 2012: (a) 120-h model SST and current with model track (blue with white circles every 24 h), model 17 m s^{-1} wind swath (white), and best track (black); (b) 6–8 Sep TMI SST with best track 17 m s^{-1} wind swath (white); (c) 120-h model SST anomaly; (d) 6–8 Sep TMI SST anomaly from 1 to 3 Sep; (e) 120-h model 77.5-m *T*; (f) as in Fig. 3f.

size forecast is up to 50–100 km larger, than the best track observations (Fig. 7f), perhaps due to the underestimation of the SST cooling throughout the forecast, which may be at least partially explained by the faster HWRF storm propagation speed relative to the best track (Figs. 7a–e).

In summary, the selected cases of Hurricanes Earl (2010), Igor (2010), Irene (2011), Isaac (2012), and

Leslie (2012) reveal that the HWRF coupled model forecasts generally capture the TC-induced cold wake but tend to underestimate the magnitude and spatial extent of the SST cooling relative to available TMI and buoy SST observations.

b. *HWRF–POM-TC subsurface ocean temperature analysis*

Fourteen quality-controlled AXBT instruments (Sanabia et al. 2013), dropped in the vicinity of Hurricane Irene during two flights [flight 1 from ~2000 UTC 26 August through ~0300 UTC 27 August (Fig. 8) and flight 2 from ~1500 UTC through ~1700 UTC 27 August (Fig. 9)], provide a unique opportunity to examine snapshots of the HWRF upper-ocean thermal structure at point locations with and without Irene's wind forcing (Fig. 5g). This area is characterized not only by the presence of the Gulf Stream—the exact location, width, and structure of which can have a significant impact on the prestorm vertical temperature profiles at the AXBT locations—but also by the complex local bathymetry (Fig. 5h), which can impact the upper-ocean response to Irene's wind forcing. Furthermore, the presence of the Gulf Stream and complex local bathymetry may magnify the potential impact of subtle errors in Irene's HWRF storm track and translation speed on the upper-ocean response. In an attempt to correct for the HWRF storm translation speed being ~6 h too slow during 26 and 27 August, a 6-h temporal offset is applied when comparing HWRF and AXBT vertical temperature profiles (Figs. 8, 9). Finally, the nearest (in space) Navy Coupled Ocean Data Assimilation (NCODA) daily temperature profiles are provided as an additional, quasi-independent data source for model analysis (Cummings 2005; Cummings and Smedstad 2013), although some of the Irene AXBT profiles were assimilated into NCODA on subsequent days (Sanabia et al. 2013), so not all of the NCODA analyses are independent of the AXBTs. It should be noted that the NCODA product has 1/6° horizontal grid spacing, and the vertical levels in the upper 200 m are defined at depths of 0, 2.5, 7.5, 12.5, 17.5, 25, 32.5, 40, 50, 62.5, 75, 100, 125, 150, and 200 m.

1) SOUTHERNMOST TEMPERATURE PROFILES (AXBTS 1, 3, 6, AND 7)

The four southernmost AXBTs are 1 (Fig. 8a), 3 (Fig. 8c), 6 (Fig. 8f), and 7 (Fig. 8g), with 1 and 6 (3 and 7) dropped in the left-rear (right rear) quadrant of Irene ~150–250 km away from the storm center between ~2000 UTC 26 August and ~0200 UTC 27 August. From before Irene's approach to the time of the AXBT drop, the HWRF upper-ocean mixed layer (OML) at AXBT 1 (3, 6, and 7) cooled from ~29.7° to ~29.2°C (from ~28.6° to ~27.6°C, from ~29.5° to ~29.2°C, and from ~28.7° to ~27.7°C, respectively) and deepened from ~25 to ~60 m (from ~20 to ~50 m, from ~25 to ~60 m, and from ~20 to ~50 m, respectively), including the 6-h offset to account for the HWRF storm translation speed error. By comparison, AXBT 1 (3, 6, and 7) indicated an OML temperature of ~28.5°C (~26.1°, ~28.7°, and ~26.9°C, respectively) and a depth of ~60 m (~50, ~60, and ~40 m, respectively). Below the OML, the HWRF and AXBT vertical temperature gradients are generally similar in the upper thermocline (down to ~200-m depth), but the anomalously warm HWRF temperature (relative to the AXBTs) continues downward from the OML to the upper thermocline). The reason for this warm bias is not clear, but it could be related to any combination of insufficient ocean model resolution, inadequate physics (e.g., mixing), and misrepresented initial temperature (and/or salinity) stratification. Storm intensity and size were not a factor here because the model storm was *stronger* and similar in size to the observed storm during this time (Fig. 5f). NCODA's temperature profiles—prestorm, in-storm, and poststorm—generally fall within the range of HWRF and the AXBT, although the NCODA OML is shallow (~20–30 m) even after Irene's forcing is applied, indicating that much of Irene's impact on the upper ocean was probably not captured by NCODA at these times and locations.

2) IMPACT OF THE GULF STREAM LOCATION (AXBTS 2, 5, AND 13)

AXBTs 2 (Fig. 8b) and 5 (Fig. 8e) were dropped to the northeast (i.e., ahead) of Irene near what appears to be the edge of the Gulf Stream at ~2100 UTC 26 August and ~0000 UTC 27 August, respectively. AXBTs 2 and 5 are therefore reasonable estimates of the prestorm ocean condition at their respective locations. The prestorm HWRF, AXBT, and NCODA profiles all agree rather well, except the AXBT has a deeper OML (~55–60 m) than the HWRF and NCODA (~35 m), and at the AXBT 2 location, the NCODA vertical temperature gradient is not as sharp as HWRF and the AXBT near the base of the OML but sharper than HWRF and the AXBT below ~100-m depth, while at the AXBT 5 location, the HWRF and NCODA vertical temperature gradient is sharper than the AXBT near the base of the OML but not as sharp as the AXBT below ~140-m depth. Hence, the AXBTs indicate that these locations may be closer to the Gulf Stream than HWRF (or NCODA) suggests; alternatively, the background ocean stratification associated with the near–Gulf Stream environment may also be misrepresented in the HWRF initial ocean condition. Poststorm, HWRF indicates

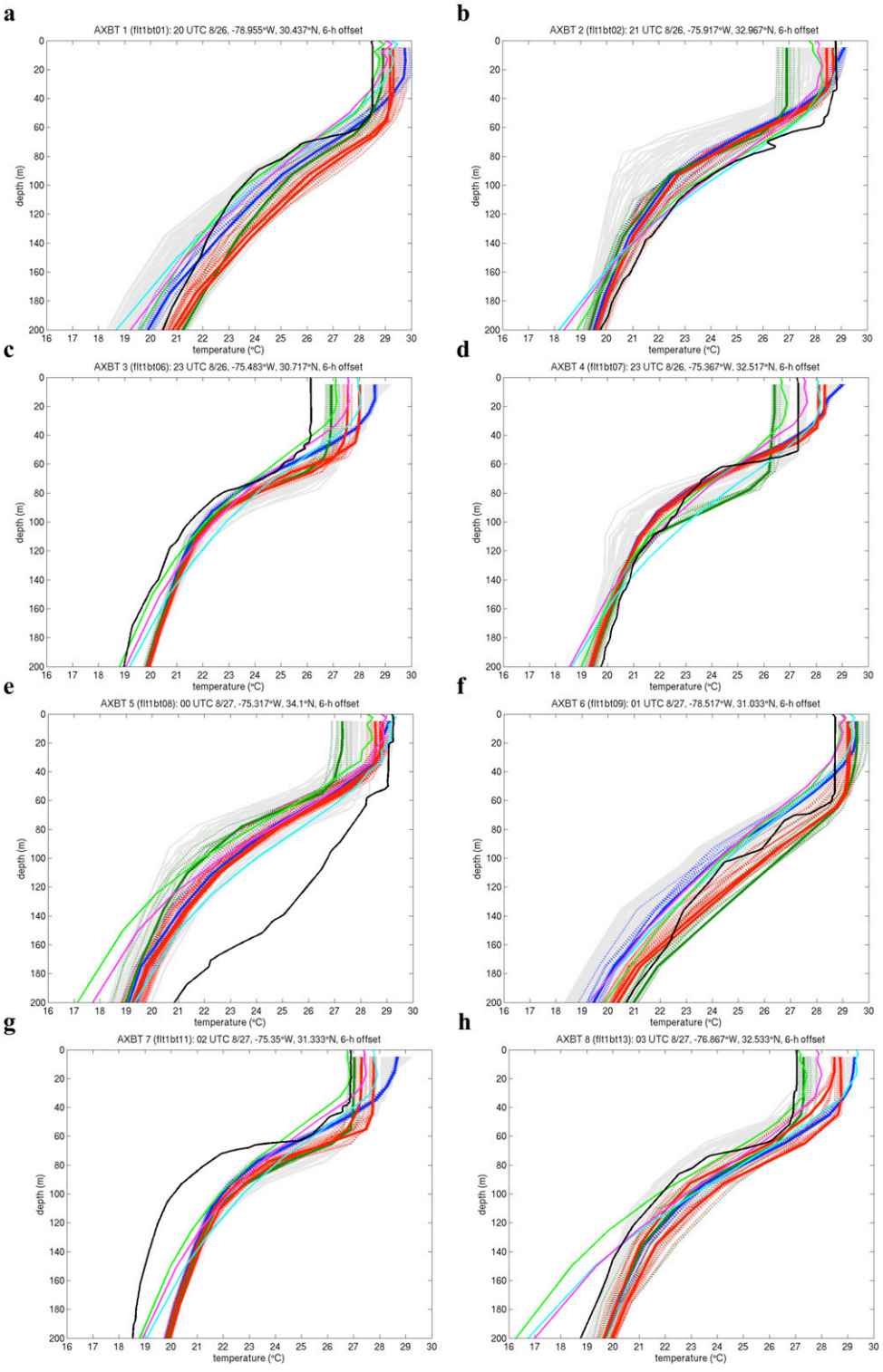

FIG. 8. Vertical temperature profiles during HWRF–POM-TC 120-h forecast of Hurricane Irene, initialized 1200 UTC 23 Aug 2011, at AXBT (a)–(h) 1–8. AXBT number (and navy flight/BT number), time, position, and offset are given in panel titles. Solid profiles are AXBT (black); all HWRF–POM-TC 6-h times, with nearby grid points (light gray); HWRF–POM-TC at 0000 UTC 26 Aug (dark blue); HWRF–POM-TC at 6-h times bounding AXBT time (red); HWRF–POM-TC at 1200 UTC 28 Aug (dark green); NCODA on 26 Aug (light blue); NCODA on 27 Aug (magenta); NCODA on 28 Aug (light green). Dotted profiles are at nearby POM-TC grid points, valid during same-colored solid POM-TC profiles.

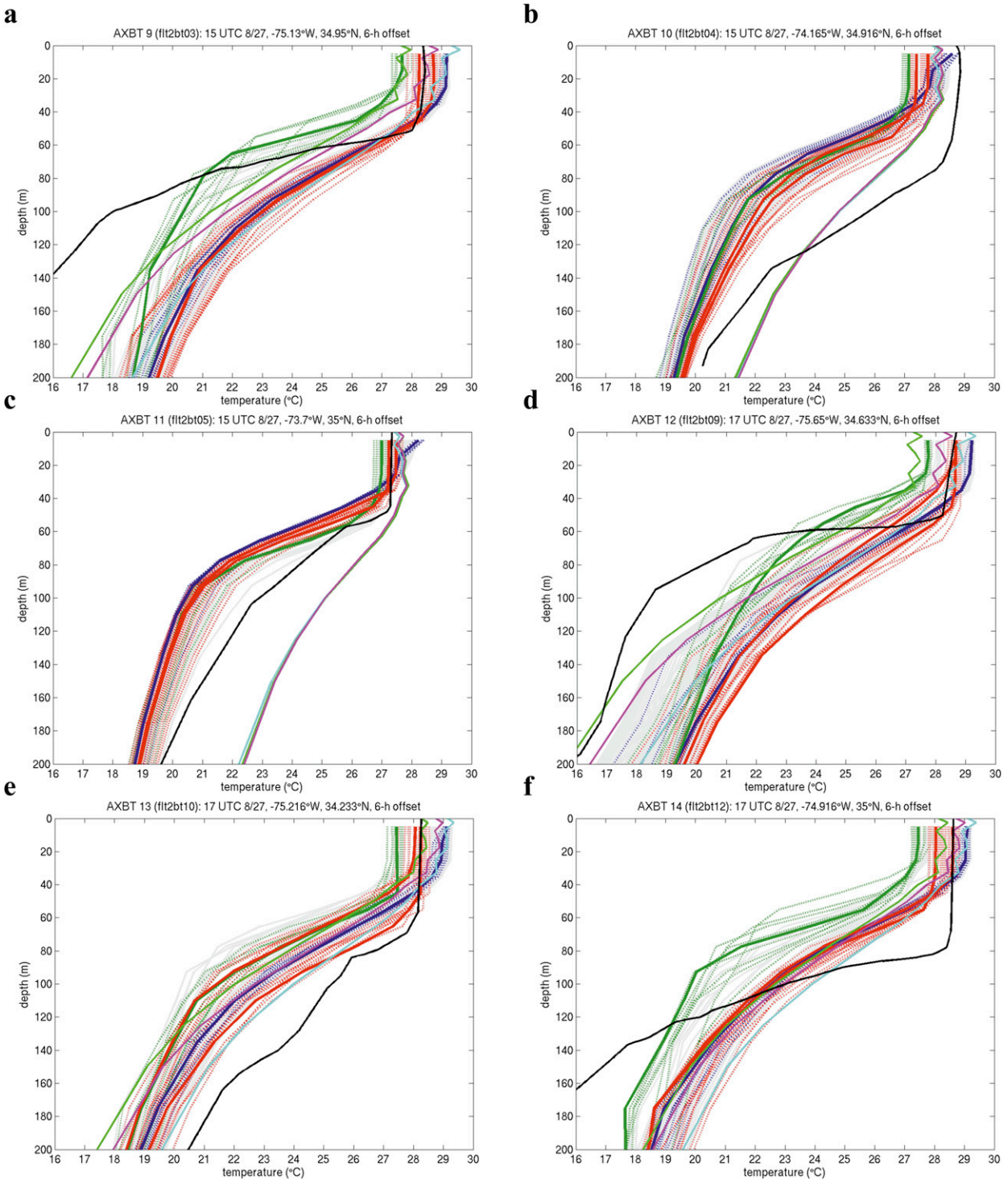

FIG. 9. As in Fig. 8, but at AXBT (a)–(f) 9–14.

~2°C of OML cooling, while NCODA indicates only ~1°C of OML cooling, but the timing of these AXBTs (i.e., prestorm) precludes their usefulness as an analysis tool for this purpose.

AXBT 13 (Fig. 9e) was dropped ~200 km to the southeast of Irene in the near-storm cold wake at ~1700 UTC 27 August. Since AXBT 13 is approximately collocated with AXBT 5 (in space, not time), it provides

a unique opportunity to compare the evolution of the upper-ocean thermal structure shortly before (AXBT 5) and after (AXBT 13) Irene's wind forcing is applied from two independent in situ observations. Comparing the HWRF, AXBT, and NCODA profiles from AXBT 13 (Fig. 9e) to AXBT 5 (Fig. 8e), it is rather clear that the main differences in the upper thermocline are due to the AXBT profile indicating that the location is in the Gulf Stream, while HWRF and NCODA indicate that the location is east of the Gulf Stream. Interestingly, HWRF indicates a high-frequency upwelling/downwelling cycle at the location of AXBT 13 (Fig. 9e, two solid red profiles), which may or may not be realistic given the eastward HWRF track bias. Nonetheless, the HWRF OML cooling agrees well with the AXBT 13 OML temperature at the time of the AXBT 13 drop (Fig. 9e).

3) PRESTORM UPPER-OCEAN COOLING (AXBTS 4 AND 8)

AXBT 4 (Fig. 8d) was dropped ~150–200 km to the east-northeast of Irene at ~2300 UTC 26 August, slightly in advance of the storm's closest approach. At that location, from before Irene's approach to the time of the AXBT drop, the HWRF OML cooled from ~29° to ~28.1°C and deepened from ~0 to ~35 m. AXBT 4 indicated an OML temperature of ~27.3°C and a depth of ~50 m, appreciably colder than HWRF but not compared to the poststorm HWRF (and NCODA) OML temperatures (~26.3°C). Nonetheless, the significant AXBT-indicated cooling *ahead* of Irene's closest approach (relative to HWRF) may have had important implications for Irene's subsequent intensity change, and in fact Irene did weaken more than indicated by the HWRF forecast prior to landfall in North Carolina (Fig. 5f), although at least part of this intensity difference may be due to errors in HWRF storm track and translation speed (Fig. 5g). While this underestimated prestorm cooling could be due to insufficient mixing in HWRF, it could also be due to underestimated along-track temperature advection of the cold wake by the Gulf Stream, similar to the scenario described for a warm ocean eddy in Yablonsky and Ginis (2013).

AXBT 8 (Fig. 8h) was dropped very close to the center of Irene at ~0300 UTC 27 August. At that location, from before Irene's approach to the time of the AXBT drop, the HWRF OML cooled from ~29.2° to ~28.6°C and deepened from ~25 to ~30–45 m (with high temporal variability, as indicated by the differences between the two solid red profiles). AXBT 8 indicated an OML temperature of ~27°C and a depth of ~55 m, consistent with the *poststorm* HWRF (and NCODA) OML temperatures (~27.2°C). Hence, the observed ocean temperature under the storm core is more representative of the cold wake than it is of the partially cooled ocean regime that might be expected directly under the storm core; this result would support the Gulf Stream–induced along-track temperature advection hypothesis discussed earlier, although ocean current observations would be required to test this hypothesis further. For both AXBTs 4 and 8, similar to the southern poststorm temperature profiles [section 3b(1)], the HWRF and AXBT vertical temperature gradients are similar in the upper thermocline, and NCODA's temperature profiles fall within the range of HWRF and the AXBT, although the NCODA OML remains shallow after Irene's forcing is applied, and the NCODA vertical temperature gradient is much sharper than both HWRF and the AXBT below ~100–150-m depth.

4) REGION OF STRONG UPWELLING (AXBTS 9, 12, AND 14)

AXBT 9 (Fig. 9a) was dropped ~150 km to the east of Irene at ~1500 UTC 27 August, at the approximate time of the storm's closest approach. At that location, from before Irene's approach to the time of the AXBT drop, the HWRF OML cooled from ~29.2° to ~28.5°C and deepened from ~30 to ~45 m. AXBT 9 indicated an OML temperature of ~28.4°C and a depth of ~55 m, similar to HWRF. Interestingly, in the upper thermocline below the OML, the AXBT (but not HWRF) has a very sharp vertical temperature gradient, leading to a temperature of ~18°C at ~100-m depth (vs ~23°C in HWRF), which suggests significant upwelling occurred at this location (assuming the AXBT is accurate). The physical mechanism for this upwelling is not immediately clear, but one possibility is strong coastal upwelling due to the wind blowing parallel to the coast (from the south), with the coast on the left, for the short period of time that includes the time of the AXBT drop. Indeed, it is plausible that the thermal structure at this location may look very different at earlier and later times when the wind is blowing from the east and west, respectively. Nonetheless, HWRF also indicates strong upwelling in the poststorm profile, but the HWRF temperature never falls below ~19°C in the upper 140 m, while the AXBT profile indicates a 140-m temperature of <16°C. NCODA's temperature profiles again fall within the range of HWRF and the AXBT, and while NCODA does indicate upwelling, it is not as significant as the upwelling indicated by the AXBT. The offshore HWRF track bias may help to explain the weaker coastal upwelling signature in HWRF compared to the AXBT.

AXBT 12 (Fig. 9d) was dropped ~100–150 km to the southeast of Irene in the near-storm cold wake at ~1700 UTC 27 August. Because of the HWRF track error, the AXBT 12 location is close to the HWRF-forecasted

storm center at this time. AXBT 14 (Fig. 9f) was dropped ~150 km to the east of Irene at ~1700 UTC 27 August, at the approximate time of the storm's closest approach and within ~15 km of AXBT 9. For brevity, the details of the AXBTs 12 and 14 profiles are not discussed further here, except to highlight that the situation is similar to AXBT 9, in which the AXBT indicates strong upwelling that is not represented as strongly in either HWRF or NCODA, except near the base of the OML in the HWRF poststorm profile. Also, the thickness of the OML, which is ~80 m according to the AXBT 14 profile (as opposed to a thickness of only ~55 m for the AXBT 9 profile), is severely underestimated by HWRF and NCODA, suggesting a combined effect of underrepresented upwelling in the thermocline and an anomalously cool initial OML temperature, perhaps due to misplacement of the Gulf Stream.

5) Region of strong downwelling (AXBTs 10 and 11)

AXBTs 10 (Fig. 9b) and 11 (Fig. 9c) were dropped ~250–300 km to the east of Irene at ~1500 UTC 27 August, at the approximate time of the storm's closest approach. At these locations, from before Irene's approach to the time of the AXBT 10 (11) drop, the HWRF OML cooled from ~28.5° to ~27.5°C (from ~28.2° to ~27.3°C) and deepened from ~0 to ~40 m. AXBT 10 (11) indicated an OML temperature of ~28.8°C (~28.3°C) and a depth of ~70 m (~50 m), significantly warmer and deeper than HWRF in the case of AXBT 10. In direct contrast to AXBT 9, in the upper thermocline below the thick OML, AXBTs 10 and 11 have a rather gradual vertical temperature gradient, leading to a temperature of ~26°C at ~100-m depth (vs ~22°C in HWRF) in the case of AXBT 10, which suggests significant downwelling occurred at this location (assuming the AXBT is accurate). The physical mechanism for this downwelling may coincide with the coastal upwelling at the location of AXBT 9, whereby eastward currents from the location of AXBT 9 create convergence and downwelling at the location of AXBT 10 (and AXBT 11, to a lesser extent), at least within the time frame of the AXBTs 9–11 drops (~1500 UTC 27 August). Interestingly, while the HWRF profiles do not indicate strong downwelling, the NCODA profiles are ~2°–4°C warmer than HWRF in the upper thermocline, suggesting that NCODA may place AXBTs 10 and 11 within the Gulf Stream, while HWRF places AXBTs 10 and 11 east of the Gulf Stream. Also, the offshore HWRF track bias may help to explain the weaker downwelling signature in HWRF compared to the AXBT.

6) Summary

In summary, the Irene (2011) AXBTs support the earlier finding that the HWRF upper-ocean mixed layer temperature does not cool as dramatically (or as quickly) as observed, but the complex bathymetry and close proximity to the Gulf Stream and the coastline make it difficult to draw strong conclusions about the performance of the POM-TC component of the HWRF from these AXBT measurements. A more in-depth analysis of the physical mechanisms responsible for the details of the observed upper-ocean AXBT temperature profiles is beyond the scope of this study, but as shown, in situ upper-ocean observations such as these provide a valuable tool for evaluating and perhaps improving the ocean component of coupled hurricane–ocean models.

4. Concluding remarks

From 2007 to 2013, POM-TC was the ocean model component of NOAA's operational HWRF, simulating the evolving SST field under TCs to facilitate accurate real-time TC intensity forecasts. Here, the 2013 operational version of HWRF is used to analyze the POM-TC ocean temperature response to five Atlantic hurricanes. The model results are compared against remotely sensed (TMI) and in situ (buoy) SST observations, when available. For the 5-day forecast of Hurricane Irene, initialized at 1200 UTC 23 August 2011, the model results are also compared to observed (AXBT) ocean temperature profiles and the NCODA product.

For the cases analyzed, the model generally underestimates the hurricane-induced upper-ocean cooling, particularly far from the storm track, as well as the upwelling and downwelling oscillation in the cold wake, compared with observations. The cooling underestimation could be due to a variety of factors. At storm's periphery, near the 17 m s^{-1} wind radius, underestimated ocean-to-atmosphere heat flux may contribute to insufficient SST cooling in the model (e.g., Vincent et al. 2012a), although heat flux measurements would be required to test this hypothesis. In the storm core, particularly in the case of Hurricane Irene, underprediction of the along-track horizontal temperature advection due to preexisting ocean currents (e.g., the Gulf Stream) may also have contributed to the insufficient model SST cooling (e.g., Yablonsky and Ginis 2013). Errors in the position and strength of ocean temperature fronts responsible for generating the preexisting ocean currents (e.g., the Gulf Stream) also contributed to errors in the prestorm background stratification, which ultimately affects the storm-induced SST cooling. In addition to background currents, storm-induced current divergence and convergence may be too weak in the model, leading to

insufficient upwelling and downwelling, but ocean current observations would be required to test this hypothesis.

Overall, underestimation of the SST cooling and subsurface ocean response may be due to a combination of coarse ocean model resolution and insufficient ocean model physics. While Vincent et al. (2012a) simulate reasonable cold wakes with an ocean model that is even coarser than POM-TC, the projection of the wind stress onto the coarse ocean model grid may cause the ocean model to miss the maximum wind forcing at certain times, leading to underpredicted SST cooling even when the storm intensity and size are well predicted in the atmospheric model (e.g., Jourdain et al. 2014; M. Kaufman et al. 2014, unpublished manuscript). The Mellor–Yamada level 2.5 turbulence closure scheme used in POM-TC may be insufficient for representing the TC-induced vertical mixing in high wind conditions; this deficiency could be addressed by including wave-dependent upper-ocean mixing or by implementing alternative vertical mixing parameterizations.

While POM-TC has its limitations, the magnitude, spatial extent, and timing of the model SST cooling are sufficient to warrant its continued use in HWRF, with major upgrades to address the known deficiencies. Starting in 2014, the operational HWRF hurricane model is expected to benefit from the replacement of POM-TC coupling with a new Message Passing Interface version of POM-TC (MPIPOM-TC; Yablonsky et al. 2015). MPIPOM-TC incorporates many of the community-based upgrades to POM from 1994 to 2012 by blending the existing version of POM-TC with a Message Passing Interface–enabled version of POM (Oey et al. 2013; Jordi and Wang 2012). MPIPOM-TC allows for higher spatial resolution and a larger domain size than POM-TC. In fact, one of the key improvements in MPIPOM-TC is the replacement of the two overlapping POM-TC domains in the North Atlantic Ocean, each of which have ~18-km horizontal grid spacing, with a single new transatlantic domain, which has ~9-km horizontal grid spacing. MPIPOM-TC is computationally efficient and scalable, and it has netCDF input/output (I/O), which is more user friendly than POM-TC's Fortran binary I/O. MPIPOM-TC has the ability to be initialized with a variety of global ocean products, including the stand-alone NCODA (Cummings 2005; Cummings and Smedstad 2013) and two versions of the Hybrid Coordinate Ocean Model (Chassignet et al. 2009) that use NCODA: NOAA's Global Real-Time Ocean Forecast System (http://polar.ncep.noaa.gov/global) and the U.S. Navy's global ocean prediction system (http://hycom.org/dataserver). Finally, MPIPOM-TC will serve as the framework for testing and perhaps implementing physics upgrades, such as wave-induced mixing and three-way atmosphere–wave–ocean coupling.

Acknowledgments. Thanks to the NOAA Environmental Modeling Center and Developmental Testbed Center HWRF teams; and thanks to Joe Cione, Eric Uhlhorn, and George Halliwell at NOAA's Atlantic Oceanographic and Meteorological Laboratory, as well as Melissa Kaufman and Tracy McCormick, who contributed to the HWRF–POM-TC analysis. Thanks to Elizabeth Sanabia at the U.S. Naval Academy for the helpful suggestions. AXBT data are provided by the U.S. Naval Academy TROPIC program and the U.S. Naval Research Laboratory (http://www.usna.edu/Users/oceano/sanbia/tropic.htm). TMI data are produced by Remote Sensing Systems and sponsored by the NASA Earth Science MEaSUREs DISCOVER Project (http://www.remss.com). Buoy data are provided by NOAA's National Data Buoy Center (http://www.ndbc.noaa.gov). The satellite-derived SSH is from Robert Leben at the Colorado Center for Astrodynamics Research (http://eddy.colorado.edu/ccar/ssh/hist_gom_grid_viewer). NCODA data are provided by the U.S. Navy's Fleet Numerical Meteorology and Oceanography Center for the Global Ocean Data Assimilation Experiment (http://usgodae.org/cgi-bin/datalist.pl?summary=Go&dset=fnmoc_glb_ocn). Finally, thanks to five anonymous reviewers, who provided helpful suggestions to improve this manuscript. This research was funded by NOAA/HFIP Grant NA12NWS4680002, awarded to the University of Rhode Island.

REFERENCES

Avila, L. A., 2002: Best track determination at NHC. Preprints, *25th Conf. on Hurricanes and Tropical Meteorology,* San Diego, CA, Amer. Meteor. Soc., 11C.1. [Available online at https://ams.confex.com/ams/25HURR/techprogram/paper_36320.htm.]

Bao, J.-W., J. M. Wilczak, J.-K. Choi, and L. H. Kantha, 2000: Numerical simulations of air–sea interaction under high wind conditions using a coupled model: A study of hurricane development. *Mon. Wea. Rev.,* **128,** 2190–2210, doi:10.1175/1520-0493(2000)128<2190:NSOASI>2.0.CO;2.

Bender, M. A., and I. Ginis, 2000: Real-case simulation of hurricane–ocean interaction using a high-resolution coupled model: Effects on hurricane intensity. *Mon. Wea. Rev.,* **128,** 917–946, doi:10.1175/1520-0493(2000)128<0917:RCSOHO>2.0.CO;2.

——, ——, and Y. Kurihara, 1993: Numerical simulations of tropical cyclone-ocean interaction with a high-resolution coupled model. *J. Geophys. Res.,* **98,** 23 245–23 263, doi:10.1029/93JD02370.

——, ——, R. Tuleya, B. Thomas, and T. Marchok, 2007: The operational GFDL coupled hurricane–ocean prediction system and a summary of its performance. *Mon. Wea. Rev.,* **135,** 3965–3989, doi:10.1175/2007MWR2032.1.

Bernardet, L., and Coauthors, 2015: Community support and transition of research to operations for the Hurricane Weather Research and Forecast Model (HWRF). *Bull. Amer. Meteor. Soc.,* in press.

Chan, J. C. L., Y. Duan, and L. K. Shay, 2001: Tropical cyclone intensity change from a simple ocean–atmosphere coupled model. *J. Atmos. Sci.,* **58,** 154–172, doi:10.1175/1520-0469(2001)058<0154:TCICFA>2.0.CO;2.

Chassignet, E. P., and Coauthors, 2009: US GODAE: Global ocean prediction with the Hybrid Coordinate Ocean Model (HYCOM). *Oceanography,* **22,** 64–75, doi:10.5670/oceanog.2009.39.

Chen, S. S., J. F. Price, W. Zhao, M. A. Donelan, and E. J. Walsh, 2007: The CBLAST-Hurricane program and the next-generation fully coupled atmosphere–wave–ocean models for hurricane research and prediction. *Bull. Amer. Meteor. Soc.,* **88,** 311–317, doi:10.1175/BAMS-88-3-311.

Cummings, J. A., 2005: Operational multivariate ocean data assimilation. *Quart. J. Roy. Meteor. Soc.,* **131,** 3583–3604, doi:10.1256/qj.05.105.

——, and O. M. Smedstad, 2013: Variational data assimilation for the global ocean. *Data Assimilation for Atmospheric, Oceanic and Hydrologic Applications,* Vol. II, S. K. Park and L. Xu, Eds., Springer, 303–343.

D'Asaro, E. A., 2003: The ocean boundary layer below Hurricane Dennis. *J. Phys. Oceanogr.,* **33,** 561–579, doi:10.1175/1520-0485(2003)033<0561:TOBLBH>2.0.CO;2.

Emanuel, K., C. DesAutels, C. Holloway, and R. Korty, 2004: Environmental control of tropical cyclone intensity. *J. Atmos. Sci.,* **61,** 843–858, doi:10.1175/1520-0469(2004)061<0843:ECOTCI>2.0.CO;2.

Falkovich, A., I. Ginis, and S. Lord, 2005: Ocean data assimilation and initialization procedure for the coupled GFDL/URI hurricane prediction system. *J. Atmos. Oceanic Technol.,* **22,** 1918–1932, doi:10.1175/JTECH1810.1.

Gentemann, C. L., F. J. Wentz, C. A. Mears, and D. K. Smith, 2004: In situ validation of Tropical Rainfall Measuring Mission microwave sea surface temperatures. *J. Geophys. Res.,* **109,** C04021, doi:10.1029/2003JC002092.

——, T. Meissner, and F. J. Wentz, 2010: Accuracy of satellite sea surface temperatures at 7 and 11 GHz. *IEEE Trans. Geosci. Remote Sens.,* **48,** 1009–1018, doi:10.1109/TGRS.2009.2030322.

Ginis, I., 2002: Tropical cyclone-ocean interactions. *Atmosphere-Ocean Interactions,* W. Perrie, Ed., Advances in Fluid Mechanics, Vol. I, WIT Press, 83–114.

——, Kh. Zh. Dikinov, and A. P. Khain, 1989: A three-dimensional model of the atmosphere and the ocean in the zone of a typhoon. *Dokl. Akad. Nauk. SSSR,* **307,** 333–337.

Hodur, R. M., 1997: The Naval Research Laboratory's Coupled Ocean/Atmosphere Mesoscale Prediction System (COAMPS). *Mon. Wea. Rev.,* **125,** 1414–1430, doi:10.1175/1520-0493(1997)125<1414:TNRLSC>2.0.CO;2.

Hong, X., S. W. Chang, S. Raman, L. K. Shay, and R. Hodur, 2000: The interaction between Hurricane Opal (1995) and a warm core ring in the Gulf of Mexico. *Mon. Wea. Rev.,* **128,** 1347–1365, doi:10.1175/1520-0493(2000)128<1347:TIBHOA>2.0.CO;2.

Huang, P., T. B. Sanford, and J. Imberger, 2009: Heat and turbulent kinetic energy budgets for surface layer cooling induced by the passage of Hurricane Frances (2004). *J. Geophys. Res.,* **114,** C12023, doi:10.1029/2009JC005603.

Jacob, S. D., and L. K. Shay, 2003: The role of oceanic mesoscale features on the tropical cyclone–induced mixed layer response: A case study. *J. Phys. Oceanogr.,* **33,** 649–676, doi:10.1175/1520-0485(2003)33<649:TROOMF>2.0.CO;2.

——, ——, A. J. Mariano, and P. G. Black, 2000: The 3D oceanic mixed layer response to Hurricane Gilbert. *J. Phys. Oceanogr.,* **30,** 1407–1429, doi:10.1175/1520-0485(2000)030<1407:TOMLRT>2.0.CO;2.

Jaimes, B., and L. K. Shay, 2009: Mixed layer cooling in mesoscale oceanic eddies during Hurricanes Katrina and Rita. *Mon. Wea. Rev.,* **137,** 4188–4207, doi:10.1175/2009MWR2849.1.

Jordi, A., and D.-P. Wang, 2012: sbPOM: A parallel implementation of Princeton Ocean Model. *Environ. Modell. Software,* **38,** 59–61, doi:10.1016/j.envsoft.2012.05.013.

Jourdain, N. C., M. Lengaigne, J. Vialard, G. Madec, C. E. Menkes, E. M. Vincent, S. Jullien, and B. Barnier, 2013: Observation-based estimates of surface cooling inhibition by heavy rainfall under tropical cyclones. *J. Phys. Oceanogr.,* **43,** 205–221, doi:10.1175/JPO-D-12-085.1.

——, B. Barnier, N. Ferry, J. Vialard, C. E. Menkes, M. Lengaigne, and L. Parent, 2014: Tropical cyclones in two atmospheric (re) analyses and their response in two oceanic reanalyses. *Ocean Modell.,* **73,** 108–122, doi:10.1016/j.ocemod.2013.10.007.

Jullien, S., and Coauthors, 2012: Impact of tropical cyclones on the heat budget of the South Pacific Ocean. *J. Phys. Oceanogr.,* **42,** 1882–1906, doi:10.1175/JPO-D-11-0133.1.

——, P. Marchesiello, C. E. Menkes, J. Lefèvre, N. C. Jourdain, G. Samson, and M. Lengaigne, 2014: Ocean feedback to tropical cyclones: Climatology and processes. *Climate Dyn.,* **43,** 2831–2854, doi:10.1007/s00382-014-2096-6.

Kim, H.-S., C. Lozano, V. Tallapragada, D. Iredell, D. Sheinin, H. L. Tolman, V. M. Gerald, and J. Sims, 2014: Performance of ocean simulations in the coupled HWRF–HYCOM model. *J. Atmos. Oceanic Technol.,* **31,** 545–559, doi:10.1175/JTECH-D-13-00013.1.

Lin, I.-I., C.-C. Wu, K. A. Emanuel, I.-H. Lee, C.-R. Wu, and I.-F. Pun, 2005: The interaction of Supertyphoon Maemi (2003) with a warm ocean eddy. *Mon. Wea. Rev.,* **133,** 2635–2649, doi:10.1175/MWR3005.1.

Liu, B., H. Liu, L. Xie, C. Guan, and D. Zhao, 2011: A coupled atmosphere–wave–ocean modeling system: Simulation of the intensity of an idealized tropical cyclone. *Mon. Wea. Rev.,* **139,** 132–152, doi:10.1175/2010MWR3396.1.

Marchok, T. P., 2002: How the NCEP tropical cyclone tracker works. Preprints, *25th Conf. on Hurricanes and Tropical Meteorology,* San Diego, CA, Amer. Meteor. Soc., P1.13. [Available online at https://ams.confex.com/ams/25HURR/techprogram/paper_37628.htm.]

Mei, W., and C. Pasquero, 2013: Spatial and temporal characterization of sea surface temperature response to tropical cyclones. *J. Climate,* **26,** 3745–3765, doi:10.1175/JCLI-D-12-00125.1.

Mellor, G. L., 1991: An equation of state for numerical models of oceans and estuaries. *J. Atmos. Oceanic Technol.,* **8,** 609–611, doi:10.1175/1520-0426(1991)008<0609:AEOSFN>2.0.CO;2.

——, 2004: Users guide for a three-dimensional, primitive equation, numerical ocean model. Program in Atmospheric and Oceanic Sciences, Princeton University, 56 pp.

——, and T. Yamada, 1982: Development of a turbulence closure model for geophysical fluid problems. *Rev. Geophys. Space Phys.,* **20,** 851–875, doi:10.1029/RG020i004p00851.

Oey, L., Y.-L. Chang, Y.-C. Lin, M.-C. Chang, F. Xu, and H.-F. Lu, 2013: ATOP—The advanced Taiwan ocean prediction system based on the mpiPOM. Part 1: Model descriptions, analyses and results. *Terr. Atmos. Oceanic Sci.,* **24,** 137–158, doi:10.3319/TAO.2012.09.12.01(Oc).

Phillips, N. A., 1957: A coordinate system having some special advantages for numerical forecasting. *J. Meteor.,* **14,** 184–185, doi:10.1175/1520-0469(1957)014<0184:ACSHSS>2.0.CO;2.

Price, J., 1981: Upper ocean response to a hurricane. *J. Phys. Oceanogr.,* **11,** 153–175, doi:10.1175/1520-0485(1981)011<0153:UORTAH>2.0.CO;2.

Reynolds, R. W., and T. M. Smith, 1994: Improved global sea surface temperature analyses using optimum interpolation. *J. Climate,* **7,** 929–948, doi:10.1175/1520-0442(1994)007<0929:IGSSTA>2.0.CO;2.

Sanabia, E. R., B. S. Barrett, P. G. Black, S. Chen, and J. A. Cummings, 2013: Real-time upper-ocean temperature observations from aircraft during operational hurricane reconnaissance missions: AXBT demonstration project year one results. *Wea. Forecasting,* **28,** 1404–1422, doi:10.1175/WAF-D-12-00107.1.

Sandery, P. A., G. B. Brassington, A. Craig, and T. Pugh, 2010: Impacts of ocean–atmosphere coupling on tropical cyclone intensity change and ocean prediction in the Australian region. *Mon. Wea. Rev.,* **138,** 2074–2091, doi:10.1175/2010MWR3101.1.

Schade, L. R., and K. A. Emanuel, 1999: The ocean's effect on the intensity of tropical cyclones: Results from a simple coupled atmosphere–ocean model. *J. Atmos. Sci.,* **56,** 642–651, doi:10.1175/1520-0469(1999)056<0642:TOSEOT>2.0.CO;2.

Shay, L. K., R. L. Elsberry, and P. G. Black, 1989: Vertical structure of the ocean current response to a hurricane. *J. Phys. Oceanogr.,* **19,** 649–669, doi:10.1175/1520-0485(1989)019<0649:VSOTOC>2.0.CO;2.

Smagorinsky, J., 1963: General circulation experiments with primitive equations. Part I: The basic experiments. *Mon. Wea. Rev.,* **91,** 99–164, doi:10.1175/1520-0493(1963)091<0099:GCEWTP>2.3.CO;2.

Tallapragada, V., and Coauthors, 2013: Hurricane Weather Research and Forecasting (HWRF) Model: 2013 scientific documentation. Developmental Testbed Center, 99 pp. [Available online at http://www.dtcenter.org/HurrWRF/users/docs/.]

Teague, W. J., M. J. Carron, and P. J. Hogan, 1990: A comparison between the Generalized Digital Environmental Model and Levitus climatologies. *J. Geophys. Res.,* **95,** 7167–7183, doi:10.1029/JC095iC05p07167.

Trahan, S., and L. Sparling, 2012: An analysis of NCEP tropical cyclone vitals and potential effects on forecasting models. *Wea. Forecasting,* **27,** 744–756, doi:10.1175/WAF-D-11-00063.1.

Vincent, E. M., M. Lengaigne, G. Madec, J. Vialard, G. Samson, N. C. Jourdain, C. E. Menkes, and S. Jullien, 2012a: Processes setting the characteristics of sea surface cooling induced by tropical cyclones. *J. Geophys. Res.,* **117,** C02020, doi:10.1029/2011JC007396.

——, ——, J. Vialard, G. Madec, N. C. Jourdain, and S. Masson, 2012b: Assessing the oceanic control on the amplitude of sea surface cooling induced by tropical cyclones. *J. Geophys. Res.,* **117,** C05023, doi:10.1029/2011JC007705.

Wentz, F. J., C. Gentemann, D. Smith, and D. Chelton, 2000: Satellite measurements of sea surface temperature through clouds. *Science,* **288,** 847–850, doi:10.1126/science.288.5467.847.

Wu, C.-C., C.-Y. Lee, and I.-I. Lin, 2007: The effect of the ocean eddy on tropical cyclone intensity. *J. Atmos. Sci.,* **64,** 3562–3578, doi:10.1175/JAS4051.1.

Wu, L., B. Wang, and S. A. Braun, 2005: Impacts of air–sea interaction on tropical cyclone track and intensity. *Mon. Wea. Rev.,* **133,** 3299–3314, doi:10.1175/MWR3030.1.

Yablonsky, R. M., and I. Ginis, 2008: Improving the ocean initialization of coupled hurricane–ocean models using feature-based data assimilation. *Mon. Wea. Rev.,* **136,** 2592–2607, doi:10.1175/2007MWR2166.1.

——, and ——, 2009: Limitation of one-dimensional ocean models for coupled hurricane–ocean model forecasts. *Mon. Wea. Rev.,* **137,** 4410–4419, doi:10.1175/2009MWR2863.1.

——, and ——, 2013: Impact of a warm ocean eddy's circulation on hurricane-induced sea surface cooling with implications for hurricane intensity. *Mon. Wea. Rev.,* **141,** 997–1021, doi:10.1175/MWR-D-12-00248.1.

——, ——, and B. Thomas, 2015: Ocean modeling with flexible initialization for improved coupled tropical cyclone-ocean model prediction. *Environ. Modell. Software,* in press.